FISEVIER

Contents lists available at ScienceDirect

# Chemical Physics Impact

journal homepage: www.sciencedirect.com/journal/chemical-physics-impact



# Full Length Article

Synthesis, structural examination, molecular interaction analysis, invitro and insilico anticancer activity investigation of a new curcumin derivative: 1-(4-chlorobenzoyl)-3, 5-bis((E)-4-methoxybenzylidene) piperidin -4-one

A. Anish Fathima <sup>a</sup>, Varuna Kumaravel <sup>b,c</sup>, D. Reuben Jonathan <sup>d</sup>, Senthil Kumar Sadasivam <sup>c,e</sup>, R. Yuvashri <sup>a</sup>, G. Usha <sup>a,\*</sup>

#### ARTICLE INFO

# Keywords: Curcumin derivative SCXRD NMR FTIR Anticancer activity In-silico investigation

#### ABSTRACT

The title material,  $C_{28}H_{24}CINO_4$ , was synthesized using the Claisen-Schmidt condensation reaction and Schotten-Baumann reaction methods and crystallized. Geometrical parameters were determined for the grown crystal using the Single Crystal X-Ray Diffraction (SCXRD) technique. The title compound has been characterized and anzalyzed for its optical properties  $via_1H^1$  and  $^{13}C$  NMR, FT-Raman, and FT-IR, UV and PL spectra. The melting point and thermal stability have been investigated using TG/DTA thermograms.Hirshfeld surfaces were developed in order to observe and quantify short contacts,  $C-H...\pi$  and  $\pi...\pi$  stacking interactions. To determine how various interactions influence the overall Hirshfeld surface, 2D fingerprint plots were created, and it was discovered that the H...H contact's contribution was the most significant. Cytotoxic effect on HEK293 cell lines was performed and found to be highly toxic. To determine the compound's efficacy as an anticancer agent, a research was conducted using MCF-7 cell lines. Molecular docking simulation revealed that the title material (ligand) fits well at the active site of the target protein with PDB ID: 1M17. Pharmacokinetic, and ADMET properties revealed that the compound is exceedingly orally active, and after further biological and pharmaceutical investigations, the compound can be recommended as a drug candidate.

#### Introduction

Natural substances acquired from fruits, vegetables, and spices, etc., have been used as prospective therapies for the majority of chronic disorders because of their non-toxic, cost-effectiveness, availability, and long-term use [1]. Curcumin is one such best example for naturally available bioactive compound that was isolated in the year 1815 [2] from the rhizomes of Curcuma longa (Zingiberaceae) [3]. It is a phytochemical molecule which is bright yellow in color The basic chemical structure of curcumin was identified in the year 1910 [4] and synthesized in the year 1913 by Milobedzka and Lampe [5]. Curcumin's molecular structure appears to be a diferuloyl methane molecule (1,7-bis

(4-hydroxy-3-methoxyphenol)—1,6-heptadiene-3,5-dione) with two ferulic acid residues connected by a methylene bridge [6]. There are various possible tautomeric forms of curucmin which includes two equivalent enol forms and 1,3- diketo form. The enol form tends to be morestable in both solid and liquid phases [7]. The biological function of numerous signaling molecules can be regulated by curcumin which is a multi-phenotypic chemical [8]. Over the years, due to extensive biological application of curucmin, there is a drastic advancement in research on curucmin [9].

Breast cancer is the second-leading cause of cancer-related fatalities globally and it is one of the most devastating types of disease that strikes women [10]. It evolves gradually, and most diseases are discovered by

E-mail address: guqmc@yahoo.com (G. Usha).

<sup>&</sup>lt;sup>a</sup> PG and Research Department of Physics, Queen Mary's College(A), Affiliated to University of Madras, Chennai-4, Tamil Nadu, India

b PG and Research Department of Biotechnology and Microbiology, National College (A), Affiliated to Bharathidasan University, Tiruchirappalli, Tamil Nadu 620001, India

<sup>&</sup>lt;sup>c</sup> Geobiotechnology Laboratory, National College (A), Affiliated to Bharathidasan University, Tiruchirappalli, Tamil Nadu 620001, India

d Department of Chemistry, Madras Christian College(A), Affiliated to University of Madras, Chennai-59, Tamil Nadu, India

e PG and Research Department of Botany, National College (A), Affiliated to Bharathidasan University, Tiruchirappalli, Tamil Nadu 620001, India

<sup>\*</sup> Corresponding author.

Fig. 1. a, 1b Chemical scheme of CMBP.

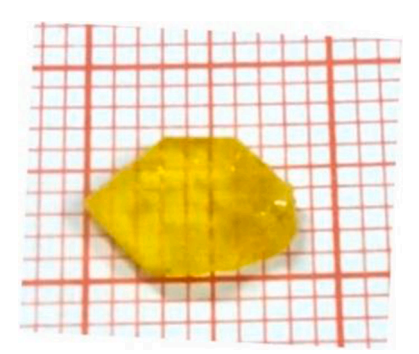


Fig. 2. Grown crystal of CMBP.

period screening. The treatment of breast cancer includes surgery (which controls local cancer), systemic therapy like chemotherapy, hormonal therapy, and targeted therapy [11,12]. The predominant chemotherapy drugs in treating breast cancer include anthracycline, doxorubicin [13], paclitaxel [14], docetaxel [15], and erlotinib [16]. Despite treating breast cancer, these drugs cause several side effects, like fertility issues, heart and nerve damage, menstrual changes, and the risk of leukemia [17]. Therefore, focusing on developing medication to treat breast cancer with no or fewer side effects is most important in current medicinal research.

The preclinical investigation demonstrates that curcumin possess high efficacy in resisting breast cancer [18]. Curcumin inhibits angiogenesis (the formation of new blood vessels) in breast cancer cells, which causes nutrient shortage and hypoxia, which leads to cell death [19]. There have been many curcumin derivatives claimed to be effective against cancer, but additional new derivatives remain a possibility, one of which could lead to best targeted epidermal growth factor receptor (EGFR) inhibitor (PDB:1M17) [20,21].

Several in-vitro and in-vivo studies on curucmin derivatives revealed that, in addition to its anti-breast cancer activity, curcumin possesses tremendous antioxidant [22–24], anti-inflammatory [25], antimicrobial [26], and anticarcinogenic [27,28] activities. Additionally, it also shows a better benefits on hepatoand nephro-protective [29,30], thrombosis-suppressing activity [31], myocardial infarction protection [32,33], and display antirheumatic effects [34]. Due to its weak water solubility and low gastrointestinal absorption, curcumin possesses a limited medicinal value [35]. To bypass this limitation, numerous

methods, including the manufacture of curcumin analogues [36,37]. These curcumin analogues are derived mainly by modifying the  $\beta$ -diketone structure and aryl substitution pattern of the molecule [38] and such derived monoketone analogues (mono-carbonyl) are more stable and water-soluble [39]. N-substituted 3, 5-bis (benzylidene) piperidin-4-one derivatives are biologically active molecules and have high potency to act as antimicrobial, antioxidant, anticancer agents, etc. [40].

To overcome the side effects of the commercially available drugs in treating breast cancer and to produce cost effective medicine, new N-substituted 3, 5-bis (benzylidene) piperidin-4-one curcumin derivative have been synthesized due to its flair biological impact. In the present study the crystallized materials structure was also elucidated. Additionally, Hirshfeld surface analysis, optical, thermal, in-vitro, and in-silico properties have been investigated and the result has been communicated.

# Materials and methods

#### Materials

All the chemicals and solvents used in this work were purchased from Sigma Aldrich and Spectrochem Pvt. Ltd., Vijaya Scientific Company, Chennai-96, Tamil Nadu, and used as such without any further purification.

# Experimental

The synthesis procedure (two steps) was carried out by following the Claisen-Schmidt condensation reaction and Schotten-Baumann reaction methods. A mixture of a 2:1 ratio of 4-methoxybenzaldehyde (0.02 mol) and 4-piperidone (0.01 mol) in the presence of 50 % NaOH along with 75 ml of ethanol was prepared, and the solution was stirred for about 3 h and kept overnight. The solution was supplemented with ice cubes to boost the precipitation. The precipitate was then filtered and kept for drying. The formed product is (Fig. 1a) 3, 5 - bis (4-methoxybenzylidene) 4-piperidone (intermediate). The mixture of intermediate product (0.01 mol), and triethylamine (0.01 mol) with 100 ml of chloroform was stirred for 2 h, and 4-chlorobenzyl chloride (0.01 mol) was added dropwise, and the solution was maintained below 10 °C. The solution was filtered and kept for evaporation to obtain the final product. The chemical scheme of the reaction is shown in Fig. 1b. The

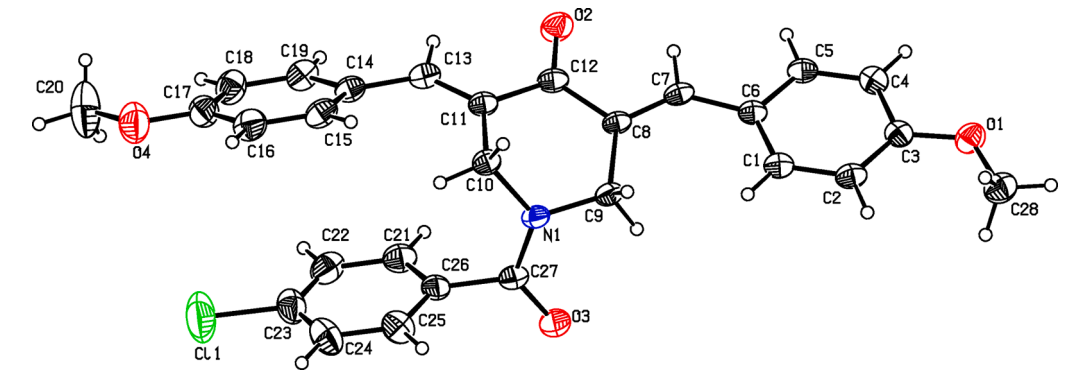
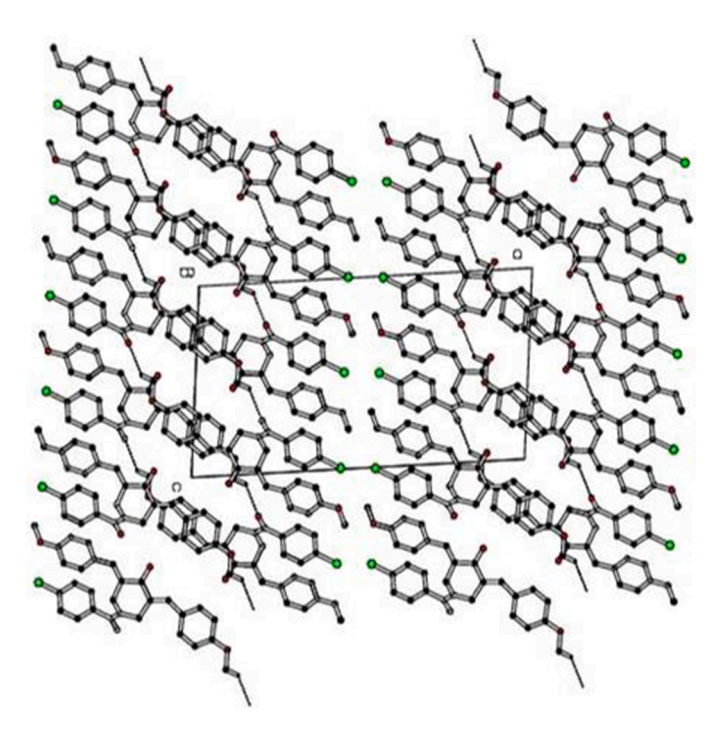


Fig. 3. ORTEP plot with numbering scheme drawn at 30 % probability level of the compound.



**Fig. 4.** Packing pattern involving dimer of the molecules in the unit cell viewed along 'b' axis. The dotted line represents the hydrogen bond.

synthesized material was then dissolved in acetone and allowed to grow by slow evaporation to get the single crystals of 1-(4-chlorobenzoyl)–3, 5-bis ((E)–4-methoxybenzylidene) piperidin-4-one [CMBP] (yield: 92 %; MP: 160  $^{\circ}$ C). The bulk crystal (Fig. 2) of the title compound was harvested after 2 weeks. The reaction mechanisms of the title synthesized material have elaborated in supplementary file (Fig. S1).

#### Chemical characterization - XRD

The crystal data were collected using a diffraction-quality crystal of size  $0.276\times0.117\times0.072$  mm using Bruker AXS kappa apex3 PHOTON II diffractometer with MoK $\alpha$  ( $\lambda=0.7107$  Å) as an X-ray radiation source from the Sophisticated Analytical Instruments Facility (SAIF), IITM, Tamilnadu, Chennai-36. The compound's structure was solved and refined using the SHELXS-97 [41], SHELXT-2014/5 [42], and SHELXL-2018/3 [43] softwares, which are interfaced on the Wingx program with the full-matrix least-squares procedure on F². The final R-factor of the title compound,  $C_{28}H_{24}ClNO_4$ , is 0.0977 with R (int) = 0.1141. The molecular graphic plots were generated using PLATON [44] and visualized using ORTEP plot [45]. The Wingx program has been utilized for determining several types of crystal's geometrical

Table 1
Crystal data collection and refinement.

COMPOUND - CMBP	
CCDC	2,184,461
Empirical formula	C <sub>28</sub> H <sub>24</sub> Cl N O <sub>4</sub>
Formula weight	473.93
Temperature	295(2) K
Wavelength	0.71073 Å
Crystal system	Monoclinic
Space group	P 2 <sub>1</sub> /c
Unit cell dimensions	a = 24.824(3)  Å
	$b = 6.9864(8) \text{ Å } \beta = 95.402(4)^{\circ}$
	c = 13.4929(16)  Å
Volume (Å <sup>3</sup> )	2329.7(5)
Z	4
Density (calculated)	1.351 Mg/m <sup>3</sup>
Absorption coefficient	$0.200 \text{ mm}^{-1}$
F(000)	992
Crystal size	$0.276 \times 0.117 \times 0.072 \text{ mm}$
DATA COLLECTION	
Theta range for data collection	3.030 to 25°
Index ranges	$-29 \le h \le 29, -8 \le k \le 8, -16 \le l \le 1$
Reflections collected	65,053
Independent reflections	4095 [R(int) = 0.1141]
Completeness to theta = 25.000°	99.80 %
Absorption correction	Semi-empirical from equivalents
REFINEMENT	
Refinement method	Full-matrix least-squares on F
Data / restraints / parameters	4095 / 0 / 309
Goodness-of-fit on F <sup>2</sup>	1.183
Final R indices $[I > 2 \text{sigma}(I)]$	$R_1 = 0.098$ , $wR2 = 0.265$
R indices (all data)	$R_1 = 0.122, wR2 = 0.285$
Largest diff. peak and hole (e. $\mathring{A}^{-3}$ )	0.55 and -0.39

parameters.Crystallographic data have been deposited with the Cambridge Crystallographic Data Center with CCDC number: 2184461.

#### Optical and thermal characterization

 $_1\mathrm{H}^1$  and  $^{13}\mathrm{C}$  NMR spectra of the grown crystal were recorded using a BRUKER ADVANCE III 500 MHz NMR spectrometer with CDCl $_3$  as a solvent. The FT-IR and FT-Raman spectrum were obtained from Bruker Optik GmbH spectrometer and BRUKER RFS 27: stand-alone FT-Raman Spectrometer, respectively. The absorbance spectrum (UV–Vis) and PL spectrum were recorded with the help of Perkin Elmer LAMBDA 950 Spectrophotometer and JY Fluorolog-3 –11 spectrofluorometer, respectively. With a temperature of up to 800 °C and a heating rate of 20 °C/min in a nitrogen atmosphere, the SDT Q600 V20.9 build 20 thermal analyzer was used to obtain TGA/DTA thermograms.

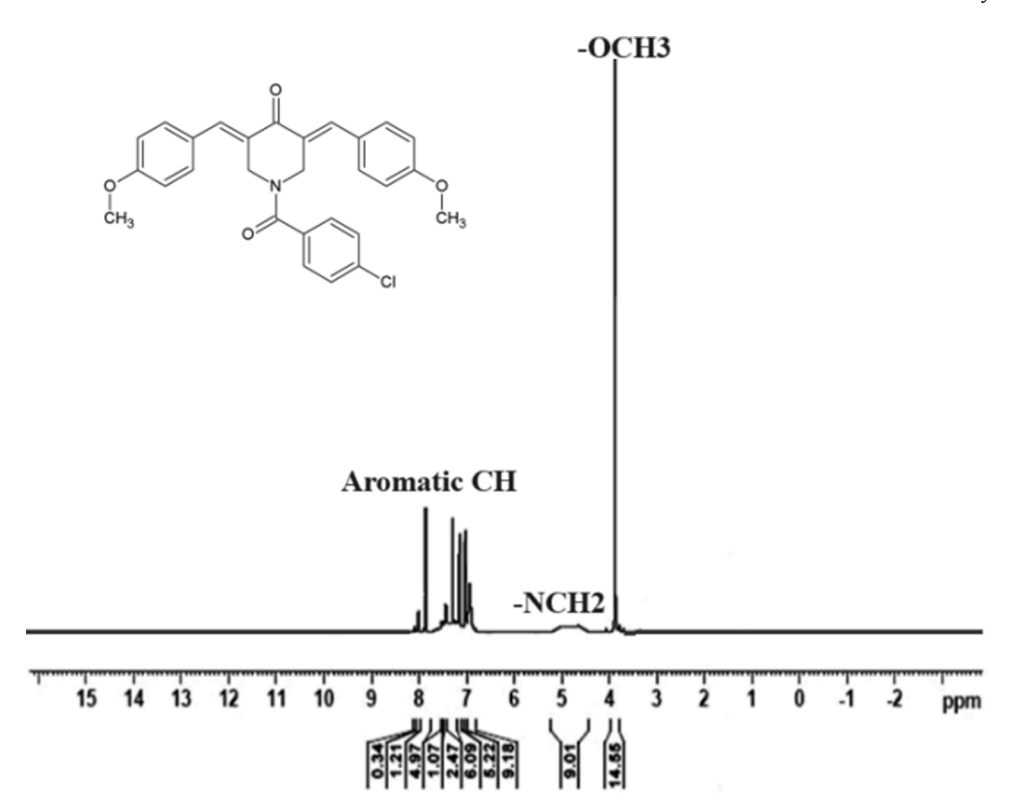
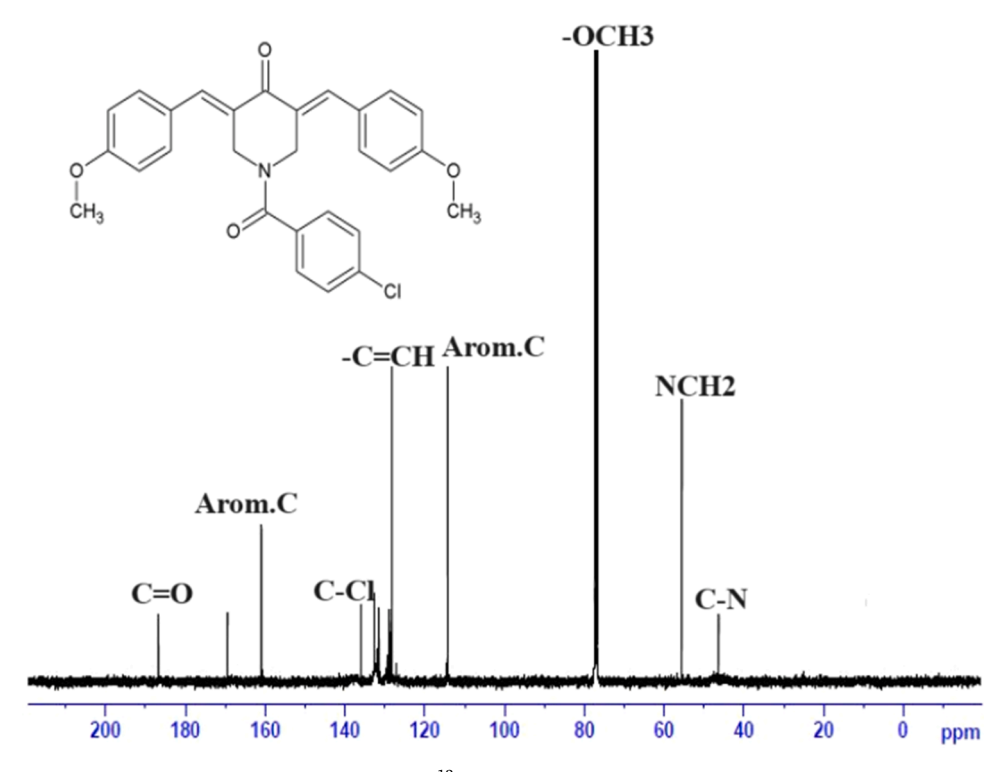


Fig. 5. 1H<sup>1</sup> spectrum of CMBP.



**Fig. 6.** <sup>13</sup>C spectrum of CMBP.

Hirshfeld surfaces and energy frameworks investigation

Hirshfeld surface (HS) analysis is a graphical tool that aids in obtaining, visualizing, and comprehending various non-covalent interactions. Molecular HS analysis and the associated 2D fingerprint plots for the compound CMBP were investigated using Crystal Explorer 17.5

program [46] by utilizing the CIF (crystallographic information files) as the input file. The normalized contact distance is

$$d_{norm} = rac{d_i - r_i^{vdW}}{r_i^{vdW}} + rac{d_e - r_e^{vdW}}{r_e^{vdW}}$$

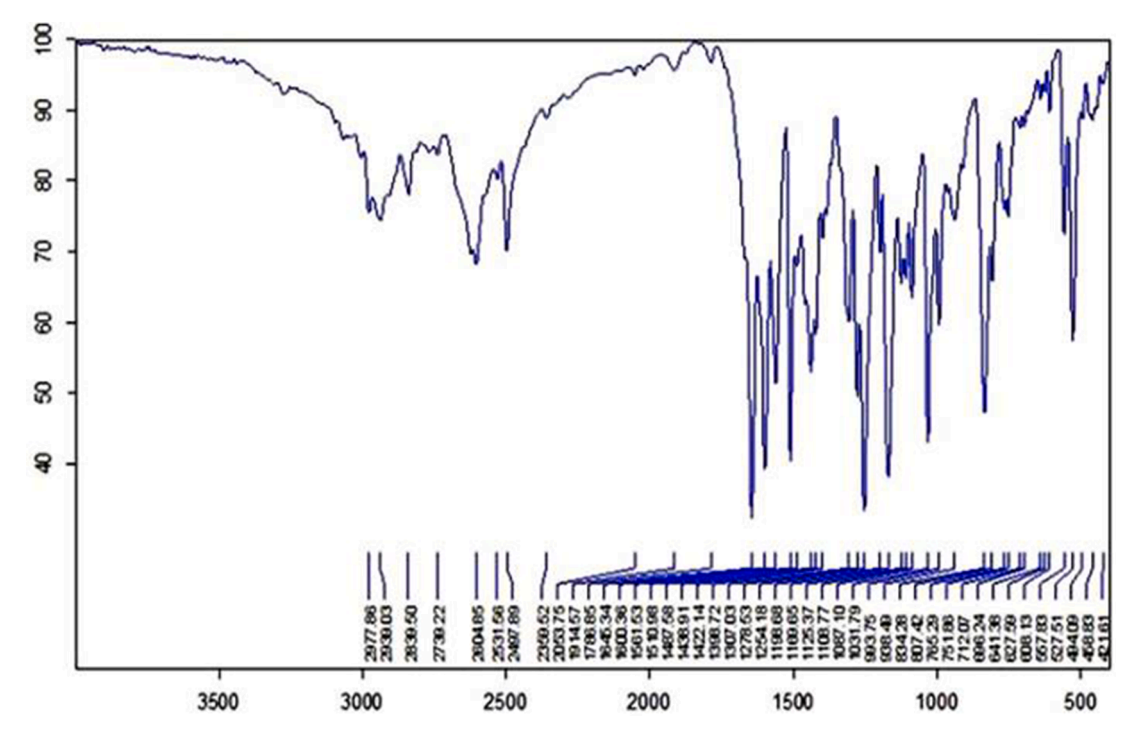


Fig. 7. FT-IR spectrum of CMBP.

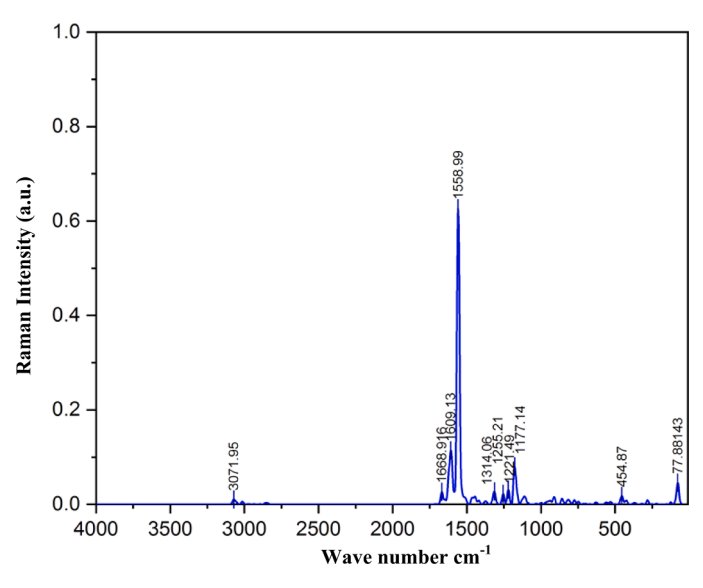


Fig. 8. FT-RAMAN spectrum of CMBP.

where  $d_e$  and  $d_i$  are the external and internal nearest nucleus distances to the surface, respectively [47]. HS plotted over the wave properties like  $d_{norm}$ , shape index, curvedness, fragment patches, and electrostatic potential (using TONTO, software incorparated into the program Crystal Explorer 17.5 [48]). 2D Fingerprint plot and Energy frame work analysis were also examined to study about the stability of the molecule.

## In-silico studies

# Molecular docking studies

Molecular docking model was performed with AutoDock 4.2.6 software package [50] and PyMOL graphic software [51]. The target protein complexed with co-crystal erlotinib (PDB ID: 1M17) [52] was acquired from the RCSB Protein Data Bank [53], and then the water molecules

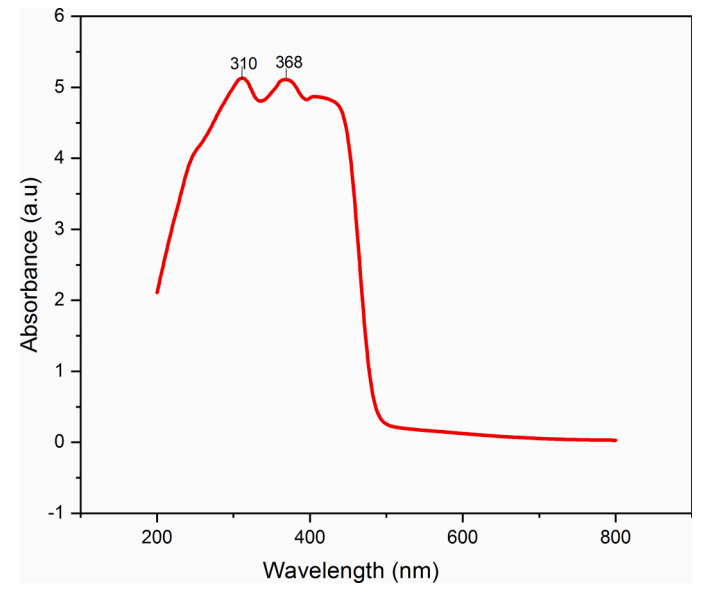


Fig. 9. UV-Vis spectrum of CMBP.

and extra side chains were removed using PyMOL software. Open Babel software is used to convert the ligand's CIF format to PDB format [54]. Polar hydrogens and Kollaman charges were added to the protein and ligand by AutoDock Tools 1.5.6 for the correction of protein structures. Docking was performed for 10 runs by the Lamarckian genetic algorithm (LGA) with  $60\times58\times60$  Å grid size along the x, y, and z-axis with grid spacing of 0.547 Å.

#### Molecular properties and pharmacokinetic prediction

A bioactive molecule's high oral bioavailability is vital for the development of the molecule as a medicinal treatment. Efficient oral bioavailability is strongly predicted by efficient intestinal absorption, reduced molecular flexibility, low polar surface area (PSA), number of

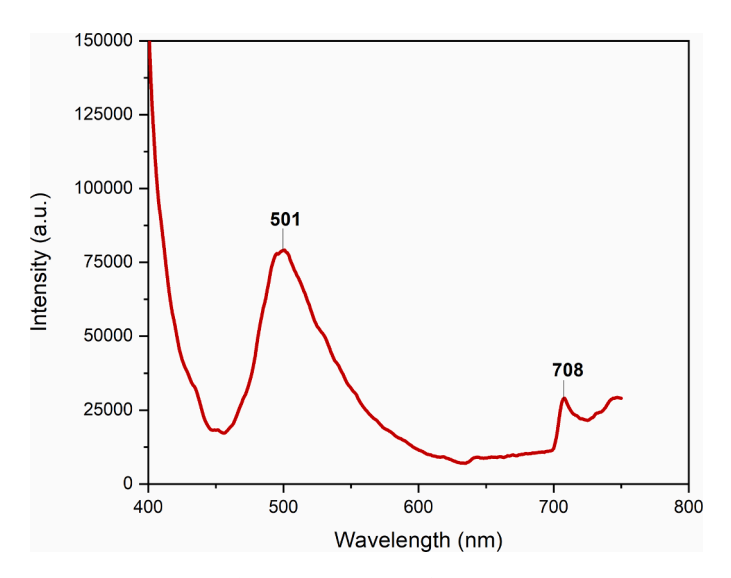


Fig. 10. PL spectrum of CMBP.

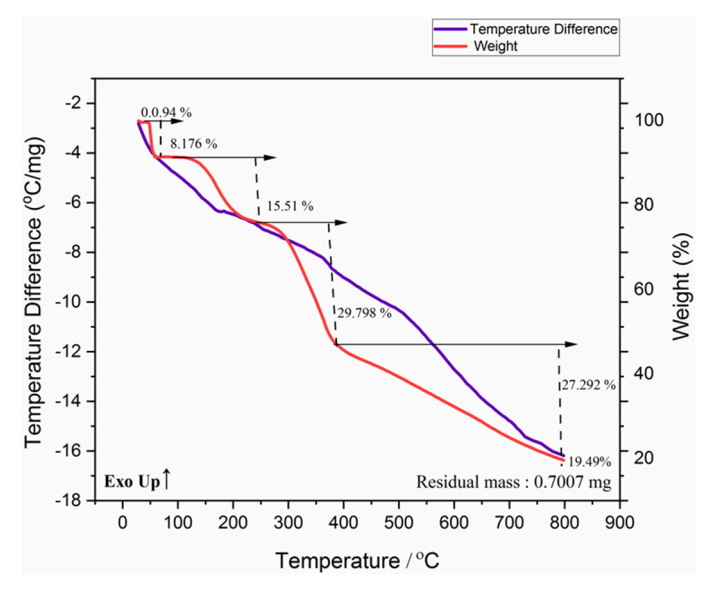


Fig. 11. TG/DTA thermogram of CMBP.

donors, number of acceptors, and number of hydrogen bonds [55]. The drug likeness of a drug candidate has been investigated using computational and structural analysis [56]. In order to calculate the compound CMBP's physicochemical characteristics and pharmacokinetic action, computational techniques were used with Molinspiration Cheminformatics [57] and the Swiss ADME web server [58].

In-vitro studies

Cytotoxcity and anticancer activity investigation

Human embryonic kidney 293 cell (normal) and MCF-7 were obtained from National Center for Cell Science (NCCS), Pune, India. The cells were cultured in Gibco Dulbecco's Modified Eagle Medium (DMEM), supplemented with 10 % fetal bovine serum (Gibco), 1 % penicillin/streptomycin antibiotics, and were incubated in a humidified atmosphere containing CO2 (5 %) at 37 °C. Cell viability was assessed by MTT assay [59]. The cells were plated at a density of  $1 \times 10^6$  cells per well in a 96-well plate at 37  $^{\circ}\text{C}$  in 5 % CO2 incubator. The cultured cells were treated with various concentrations of the samples, followed by incubation for 24 h. After 24 h incubation, 100 µl of DMEM media with MTT dye solution (5 mg/ml in phosphate buffer pH 7.4) was added to each well. After 4 h of incubation at 37 °C and 5 % CO2, the medium was removed, and formazan crystals were solubilized with 100 µl of DMSO and the solution was vigorously mixed to dissolve the reacted dye. The absorbance was measured at 570 nm using a 96-well plate reader (Bio-Rad, iMark, USA). The concentration required for 50 % inhibition (IC50) was determined graphically. The relative cell viability (%) related to control wells containing cell culture medium was calculated by the following formula:

% of cell viability = 
$$100 \text{ x} \frac{\text{Sample absorbance}}{\text{Control absorbance}}$$

#### Results and discussion

Geometrical parameters

The ORTEP [45] plot is shown in Fig. 3. The title compound,  $C_{28}H_{24}ClNO_4$ , is centro-symmetric and crystallized in a monoclinic crystal system with P  $2_1/c$  space group. The compound includes three aromatic rings (C1-C6, C14-C19, and C21-C26) and one aliphatic ring (N1/C8-C11, piperidone). The aromatic rings are bridged with the central piperidone moiety through C=C (olefinic bond) and C=O (carbonyl bond). The calculated geometrical parameters are in good agreement with similar structure [60–63]. The title material adopts E-configuration with respect to the double bonds in the interlinking olefinic chain (C7 = C8 & C11 = C13).

The central piperidone ring (N1/C8-C12) takes a distorted half-chair conformation (Fig. S2) with ring puckering parameter;q2=0.4409 (0.0045)Å,q3= -0.2724(0.0046)Å, phi2 =  $-150.51(0.63)^{\circ}$ , QT= 0.5182(0.0045)Å and Theta2= 121.71(0.51) [64]. In the crystal packing, the adjacent molecules are linked through a pair of C—H...O hydrogen bonds (Table S6, Fig. 4), forming an inversion dimer described by a graph set motif  $R_2^2[(26)]$  [65].The crystal data collection and refinement details are given in Table 1. The selected bond lengths, bond angles, torsion angles, LSQ plane details and dihedral angles between the planes are listed in S1–S5.

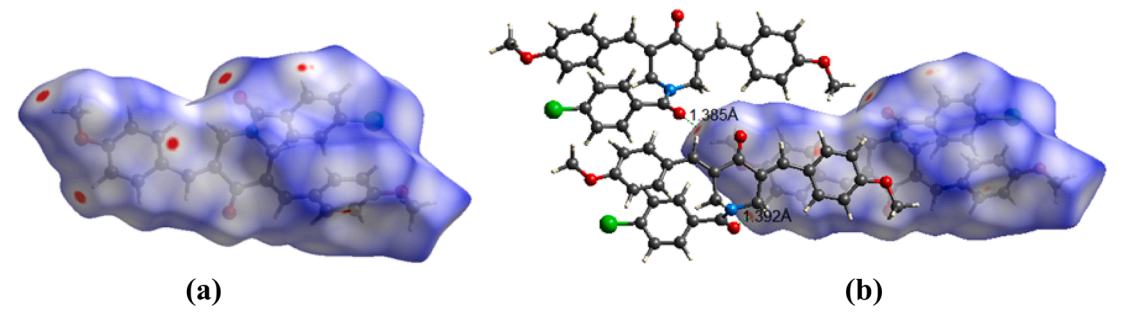


Fig. 12. [a] Hirshfeld surface mapped over dnorm and [b] showing the possible intermolecular Interactions.

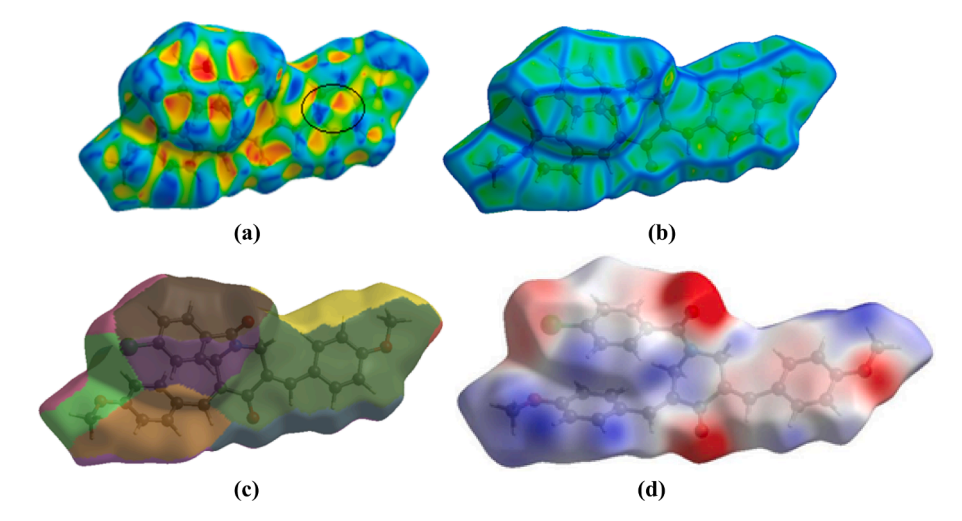


Fig. 13. Hirshfeld surfaces mapped over (a) Shaped Index (b) Curvedness (c) Fragment patches (d) Electrostatic Potentials.

Table 2
Calculated Interaction Energies for CMBP using B3LPY/6–31G(d, p) Model.

N	Symop	R	E <sub>ele</sub>	$E_{\rm pol}$	E <sub>dis</sub>	E <sub>rep</sub>	E <sub>tot</sub>
1	-x, -y, -z	10.93	-7.8	-5.3	-21.4	14.7	-21.8
2	-x, y + 1/2, -z + 1/	11.38	-23.1	-5	-83.3	56.1	-66
	2						
1	-x, -y, -z	14.40	-18.3	-7.8	-31.3	27.9	-35.2
2	x, -y + 1/2, z + 1/2	7.29	-12.9	-4.6	-58.3	33.6	-47.2
2	x, y, z	6.99	-4.8	-1.5	-22	7.8	-20.5
2	x, -y + 1/2, z + 1/2	7.96	-7.7	-4.5	-31	15.8	-28.7
1	-x, -y, -z	14.45	4.6	-0.8	-14.1	5.9	-4.3
2	-x, y + 1/2, -z + 1/	16.77	-4.4	-0.9	-10.4	5.4	-11.1
	2						
Ene	Energy Model				$k_{pol}$	$k_{dis}$	$k_{rep}$
	B3LYP B3LYP/6–310 ensities	1.057	0.74	0.871	0.618		

#### Optical and mechanical characterization

# <sub>1</sub>H<sup>1</sup>NMR and <sup>13</sup>C NMR analysis

The  $_1\mathrm{H}^1$  NMR and  $^{13}\mathrm{C}$  NMR spectral analyses have been carried out in the liquid state to analyze the presence of various types of proton and carbon atoms of the title molecule with CDCl $_3$  as a solvent. Figs. 5 and 6 display the  $_1\mathrm{H}^1$  NMR and  $^{13}\mathrm{C}$  NMR spectra of the crystal, and the chemical shifts are shown in  $\delta$  ppm and are tabulated in S7 and S8. In  $_1\mathrm{H}^1$  NMR, a strong singlet present at 3.871 ppm is attributed to the OCH $_3$ – (6H) protons present in the terminal aromatic rings [66]. The presence of -NCH $_2$  (4H) protons of piperidone moiety is observed at 4.659 and 4.978 ppm [67]. The existence of - C=CH (2H) protons are observed in the range 7.426–7.534 ppm [68]. The aromatic protons in the phenyl ring (12H) are observed in the range 6.934–8.031 ppm [66].

In  $^{13}$ C NMR, peaks at 186 ppm, 131 -132 and 114–169 ppm are ascribes to carbonyl carbon (C=O), $\alpha$ ,  $\beta$  unsaturated carbonyl carbon (C=C), and aromatic carbon, respectively [67]. The peak at  $\delta$  136 ppm is attributed to the C—Cl attached with the aromatic ring [69]. Multiplets between  $\delta$ 76.74– $\delta$ 77.38 ppm are due to the presence of methoxy carbon (OCH<sub>3</sub>–) attached to the aromatic ring [70]. A Peak at  $\delta$ 55 ppm corresponds to the carbon present in NCH<sub>2</sub> [67]. A distinct peak at  $\delta$  46 ppm is due to the presence of C—N in the piperidinone ring [69].

## FT-IR and FT-RAMAN analysis

The FT-IR and FT-RAMAN spectra of CMBP were recorded in solid form to analyze the various types of stretching and bending vibrations present in the title material and are shown in Figs. 7 and 8, respectively. The assigned frequencies are listed in S 9. A weak signal at  $3071~{\rm cm}^{-1}$  in the FT-Raman spectrum represents the aromatic C—H stretching

vibration [71], which is imperceptible in the IR spectrum due to highly substituted and condensed in nature [72]. In the IR spectrum, the weak peaks in the region 2977 and 2939 cm<sup>-1</sup> can be accounted for C-H asymmetric and symmetric stretching vibrations of CH2 group respectively [73]. From the IR spectrum, the peak around 2839 cm<sup>-1</sup> can be accounted for the CH3 stretching vibration [74]. The existence of the conjugated keto group C=O are observed as a strong peak of stretching vibration at 1645 and 1668 cm<sup>-1</sup> in IR and FT-Raman, respectively [75, 76]. The strong band around 1600 cm<sup>-1</sup>in IR and the weak band around 1609 cm $^{-1}$  in FT-Raman are attributed to – C=C group in  $\alpha$ ,  $\beta$ -unsaturated carbonyl group [76,77]. In the IR spectrum, the strong and weak peaks at 1561and 1438 cm<sup>-1</sup> and long sharp peak at 1558 cm<sup>-1</sup> in Raman spectrum are attributed to the aromatic C=C stretching vibration of the aromatic ring [78]. In the Raman spectrum a peak at  $1314 \text{ cm}^{-1}$ attributes to the -CH2 twisting vibration of the grown crystal [79]. The medium signals in the region 1278-1307 cm<sup>-1</sup> and 1255-1220 cm<sup>-1</sup> in FT-IR and FT-Raman, respectively, is due to the occurrence of C-N stretching vibration of the piperidone moiety [80.81]. In IR spectrum the presence of C - O stretching vibration is observed at 1254 cm<sup>-1</sup> [82]. In Raman spectrum C - O - C asymmetric stretching of the methoxy group attached to the aromatic ring is observed around 1177 cm<sup>-1</sup> [83]. The aromatic C—H in plane bending was observed as medium to strong peaks around 1125–1031 cm<sup>-1</sup> and C—H out of plane bending appears in the region  $970-650 \text{ cm}^{-1}$  [74]. The weak absorption signal at 696  $cm^{-1}$  represents = C—H aromatic bending vibration [84]. The C - Cl stretching vibration is observed as strong to medium peaks in the region 840-505 cm<sup>-1</sup> in IR and at 454 cm<sup>-1</sup> in FT- Raman [85,86].

## UV visible spectral analysis

The absorption spectrum of the title compound is shows in Fig. 9. The spectrum consist of two finger print peaks at 310 and 368 nm, corresponds to  $\pi$ -  $\pi^*$  electron transition which might be due to the presence of C=C and C=O groups of the title compound [87]. The band gap energy of the compound CMBP has been calculated using  $E_g=h\nu~(\lambda_{max}=368~nm)$  and was found to be 3.38 ev.

#### Photoluminiscence spectral analysis

The Photoluminescence spectrum of the grown crystal has been shown in Fig. 10. The studies exhibit two excitation peaks. The first peak is at 501 nm (Green light emission) corresponds to the fluorescence and the second peak is at 708 nm (red emission) which corresponds to phosphorescence. The emission energies of the synthesized compounds were found to be  $2.47~{\rm eV}$ .

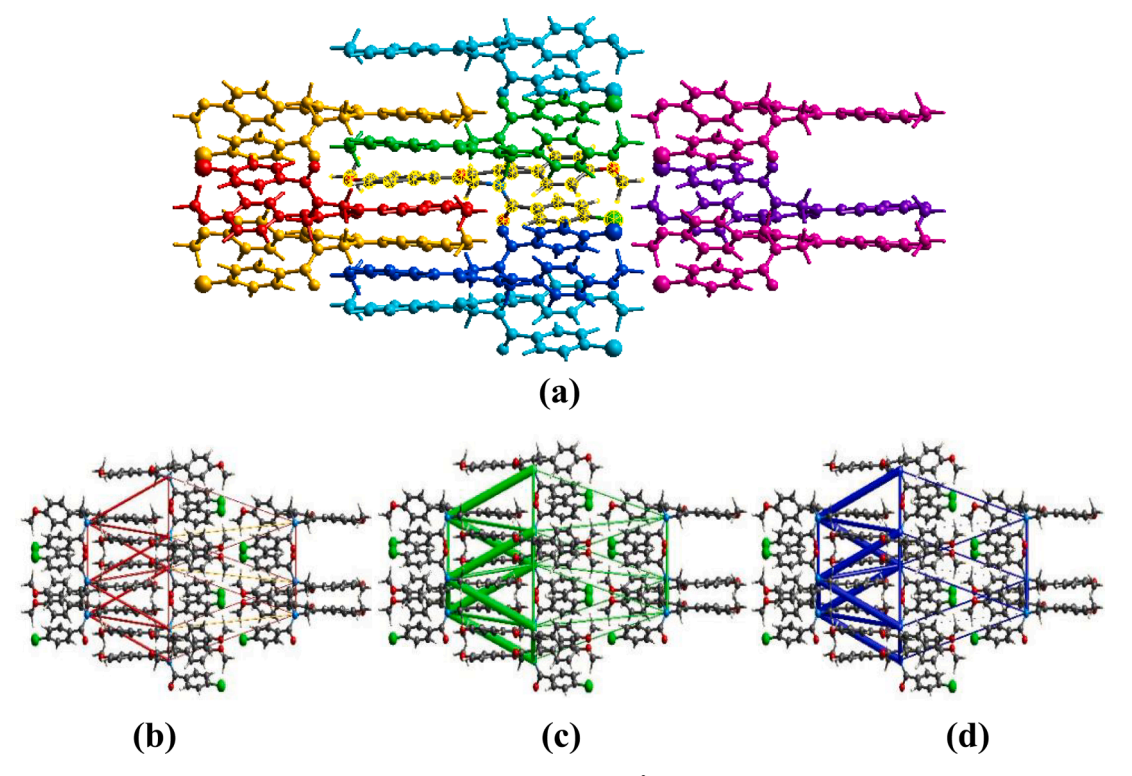


**Fig. 14.** a) Interaction between the selected molecule and the molecules present in a 3.8 Å cluster (b) Electrostatic energy (c) Dispersion energy and (d) Total energy.

#### TG/DTA

In order to analyze the stability of the material thermogravimetric and differential thermal analysis thermograms were plotted simultaneously and displayed in Fig. 11. The initial weight of the compound used for the analysis is 4 mg. The TG curve displays four stages of the decomposition process, in which the weight loss up to 76.35°C is ascribed to the desorption of the trapped water component in the material. The second stage of decay, which is up to 249.4°C is due to sublimation, in which stray solvents are converted to steam. Subsequent two stage weight loss between 249.4 and 799.7°C is due to the degradation of the title compound CMBP [88]. The presence of several ring systems and a halogen atom (Cl) linked to the aromatic ring may be accountable for the compound's high residual mass of 19.49 %. In the DTA graph a small peak at 173.80°C corresponds to the melting point of the compound. From the DTA graph it is observed that the thermal processes (exo and endo) associated with the material are negligible [89].

#### Hirshfeld surfaces analysis and energy frameworks investigation

The Hirshfeld surface was visualized for several surface properties. The  $d_{norm}$  (Fig. 12a) is a normalized contact distance, which was examined using red-blue-white scheme of colors [90]. The weak intermolecular interactions and short contacts present in the structure have been visualized, and the possible interactions between the two adjacent molecules involving the C—H...O hydrogen bond with H...A distance equals to 1.385 Å and 1.392 Å, is shown in Fig. 12b.

The neighboring red and blue triangles in the shape-index map (Fig. 13a) denote the presence of C—H- $\pi$  interactions. [91]. The  $\pi$ - $\pi$  stacking can be visualizedas the flat regions over the curvedness surface (Fig. 13b). The proximity of the nearby molecules has been examined in the fragment patches (Fig. 13c). The chemical CMBP has a coordination number of 13.On the electrostatic potential surface (Fig. 13d), the red color spots show the negative electrostatic potential (hydrogen bond forming region) and the blue color attributes to the positive electrostatic

potential [92].

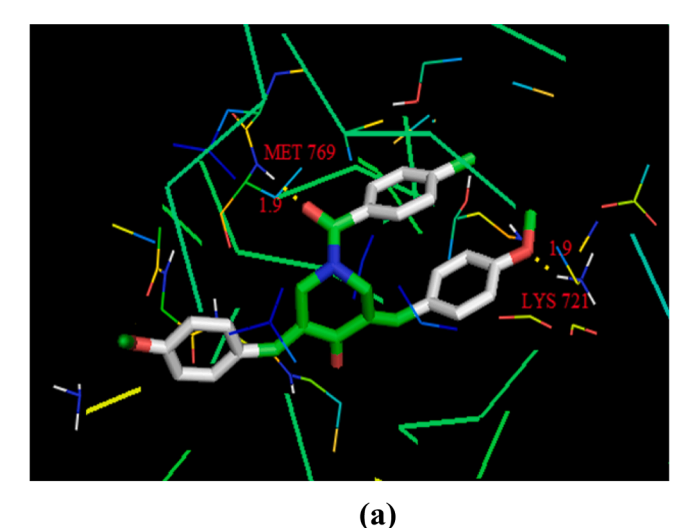
The 2D fingerprint plots (Fig. S3) helps to understand the contribution of various elemental interactions present the compound. It reveals that the H...H interactions have the largest contribution to the total Hirshfeld surface of 47.2 %. The O...H/H...O interactions with 18.6 % contribution is represented by two sharp spikes with a slight separation, and the same has been validated from the interactions generated from Platon software [44]. The existence of C...H/H...C interaction with 17.6 % reveals that the compound possesses a C—H... $\pi$  interaction which is also been confirmed by the presence of red and blue triangles in shape index. The Cl...H/H...Cl (7.1 %) and C...C (5.1 %) are the next greatest contributors to the surface contacts. The contribution percentages of other intermolecular contacts are less than 5 % in the Hirshfeld surface mapping. The large number of H...H, O...H/H...O and C...H/H...C interactions suggest that van der Waals interactions and hydrogen bondings play the major roles in the crystal packing [93].

The total intermolecular interaction energy ( $E_{tot}$ ) is the sum of four energy terms: electrostatic ( $E_{ele}$ ), polarization ( $E_{pol}$ ), dispersion ( $E_{disp}$ ), and repulsion ( $E_{rep}$ ) with scale factors of 1.057, 0.740, 0.871 and 0.618, respectively [49]. The interaction energies have been calculated for the compound using the CE-B3LYP/6–31 G (d,p) quantum level of theory, as available in Crystal Explorer is shown in Table 2, revealing that the dispersion energy is more significant than other energies. The energies between the molecular pairs around the selected molecule are shown as cylinders connecting centroids are shown in Fig. 14a-d, electrostatic energy (coulomb) by red cylinders, dispersion energy by green cylinders, and total energy by blue cylinders.

#### In-silico studies

## Molecular docking studies

The AutoDock 1.5.6 tools have attempted ten runs, which assist in obtaining the best fit interaction indicated by the lowest binding energy. Table S 10 contains the values for the scoring functions. The inhibition constant (Ki) for 1M17 with the ligand interaction was found to be 2.45



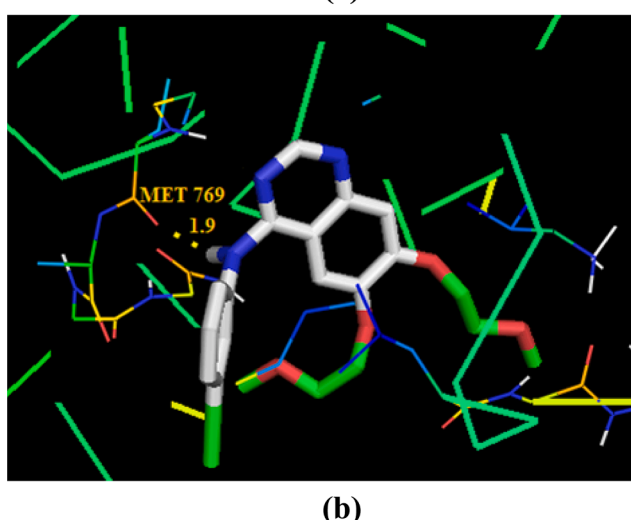


**Fig. 15.** PyMOL plot representing the interactions between (a) The ligand (CMBP) and the protein (1M17) (b) Co-crystal (Erlotinib) and the protein (1M17).

nM for run 1, which is the measure of the ligand binding affinity to the target protein. The value of Ki is directly proportional to the dosage of medication needed to stop the deadly action [94]. The ligand interaction with the 1M17 protein exhibits a lower binding energy value of  $-11.75\,$  kcal/mol during run 1. The interaction between the ligand and the target molecules is sped up by the decreased binding energy, which also suggests an increase in molecular stability [95].The title compound CMBP fits well into the active site of 1M17 protein, with N—H...O hydrogen bonds at a distance of 1.9 Å with the amino acid residues Met 769 and Lys 721(Fig. 15a). The amino acid residue Met 769 is involved in the

active site interactions of the co-crystal (Erlotinib) (Fig. 15b), which is used as a drug for treating breast cancer. Binding energy, binding site interactions, and donor-acceptor distances were listed in Table 3. Correlating the results, the title compound exhibits better binding energy and active site interactions involving the same amino acid residue as that of the complexed co-crystal (erlotinib), hence, the title molecule can be recommended as a lead candidate to design new drugs to treat breast cancer.

## In-silico molecular properties and pharmacokinetic prediction

For the title compound CMBP, all the parameters of Lipinski's RO5 (Table 4) were in the optimum range except miLogp, which is slightly greater than 5, which shows moderate permeability across the cell membrane [56]. The bioavailability rating forecasts the proportion of an oral substance that enters systemic circulation. The title compound correlates well with the bioavailability score (0.55) indicates an excellent compound for systemic circulation [96]. For a drug to be orally active, it should have high gastrointestinal absorption (GIA). CMBP exhibited high GI absorption and was permeable to the blood-brain barrier (BBB). The synthetic accessibility scores refer to how easily a compound can be synthesized in a lab, and scales of easy to hard range between 0 and 10, and was found to be 3.22, indicates that it may be produced on a wide scale with ease [95]. The lipophilicity value is 4.77, which indicates poor permeation rates across the skin [97]. Molar refractivity defines the drug's transport and bio-distribution behavior, which should be  $\leq 130$ , but for the compound CMBP it is around 137 which show poor bio-distribution [98]. The pharmocochemical

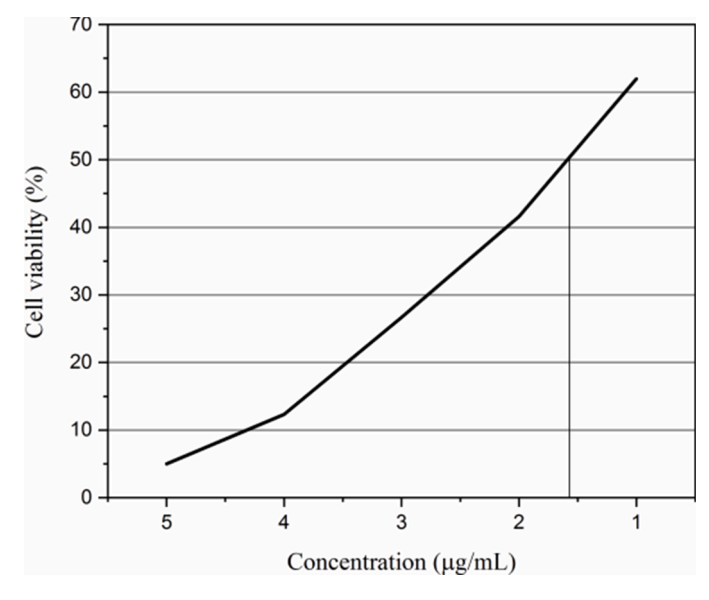


Fig. 16. Concentration vs. Cell viability plot showing the IC50 value for the title compound.

**Table 3**Binding site interactions and binding energies.

Ligand	Receptor (PDB ID)	Run Number	Binding Site Interaction	D-HA (Å)	Binding Energy kcal/mol	Inhibiton constant (ki) nM
CMBP	1M17	1	[MET' 769] N-HO	1.9	-11.75	2.45
			[LYS' 721] N-HO	1.9		
ERLOTINIB		10	[MET' 769] N-HO	1.9	-9.84	61.63

**Table 4**Drug likeness score of the compound CMBP.

miLogp	TPSA	nAtoms	nON	nOHNH	nrotb	volume	MW	nviolation
5.3	55.85	34	5	0	5	419.83	473.96	1

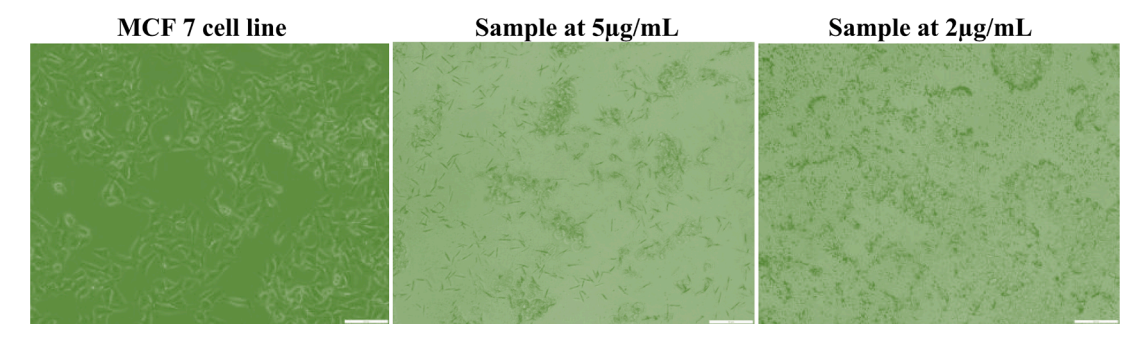


Fig. 17. Surface morphology Changes on MCF-7 Cell lines for the title Compound.

properties were tabulated in S11. Based on the aforementioned activity defining parameters, it can be concluded that the title material exhibits moderate oral bioactivity.

#### In-vitro studies

#### Anticancer and cytotoxic activity analysis

The anti-cancer activity of the synthesized compound on MCF-7 cell lines was evaluated using an MTT assay method [61]. It is observed that the cell viability decreases as the concentration of the sample increases (Table S12). The concentration corresponding to IC $_{50}$  value of the compound is around 1.6  $\mu$ g/mL (Fig. 16), which demonstrates its efficacy as potential anticancer material in the field of drug designing. MCF-7 cell treated with the synthesized compound is shown in Fig. 17.

Similarly, the cytotoxicity of the compound was done on HEK293 cell line by MTT assay method [61] and concentration vs. cell viability plot and the surface morphology are shown in Fig. S 4&5. Cytotoxicity is inverse to cell viability (Table S13), the IC $_{50}$  value of the compound is around 1.9  $\mu$ g/mL which shows that the compound is highly toxic, this may be due to environmental stress while testing and the solvent used (chloroform) during synthesis procedure. The IC $_{50}$  value corresponds to lower sample concentration (S12 & 13) clearly illustrates the title molecule is highly active against cancerous cells and shows toxicity on normal cells. In future after optimizing the toxic level on the normal cells, the compound CMBP can be considered as a drug candidate to fight against breast cancer.

#### Conclusion

A new curcumin derivative CMBP has been synthesized and it was studied for its 3D structure and crystallographic parameters using the Xray diffraction technique. The compound was crystallized in monoclinic crystal system with the space group P 2<sub>1</sub>/c. The piperidone ring adopts distorted half chair conformation. In the crystal structure, the neighbouring molecules are linked through a pair of C—H...O hydrogen bonds forming inversion dimer. The obtained crystal was characterized and analyzed using NMR, FTIR and FT Raman spectral analysis and the derived results matched well with the similar reported structures. The preferential absorption and emission signals were studied using UV/PL spectral analysis. The TG/DTA thermal studies reveal multistage decomposition of the material with high residual mass of 19 %. The non covalent interactions namely C—H-π, π-π, van der Waals, and hydrogen bonds have been visualized and analyzed via the Hirshfeld surfaces investigation. The effect of dispersion energy on the stability of the compound is verified by Energy Frame work analysis. The suitability of the title molecule for pharmacological application has been verified by performing in-silico analysis. The ligand CMBP binds well with the target protein (1M17) and shows better binding energy than the reference material (Erlotinib). The in-silico molecular and pharmacokinetic prediction shows moderate oral biovailability of the compound. An excellent anticancer activity of the compound on breast cancer cell line (MCF-7) was observed with the IC  $_{50}$  value  $<2~\mu g/mL$  but highly toxic (IC $_{50}$  value = 1.6 µg/mL) on normal cell line. Over viewing the results the newly synthesized title compound shows better in-vitro and in-silico bioactivity, in future further investigations needed to reduce the toxic level of the compound so that it can be as a drug candidate to fight against breast cancer.

#### **Funding source**

This research did not receive any specific grant from funding agencies in the public, commercial, or not-for-profit sectors.

#### CRediT authorship contribution statement

A. Anish Fathima: Writing – original draft, Formal analysis, Data curation, Conceptualization. Varuna Kumaravel: Resources. D. Reuben Jonathan: Methodology. Senthil Kumar Sadasivam: Project administration. R. Yuvashri: Software. G. Usha: Writing – review & editing, Validation, Supervision.

# Declaration of competing interest

The authors declare that they have no known competing financial interests or personal relationships that could have appeared to influence the work reported in this paper.

# Data availability

Data will be made available on request.

## Acknowledgement

The authors thank the Central Instrumentation Facility (DST– FIST), Queen Mary's College (A), Chennai-4 for the computing facility, SAIF, IIT, Madras, for the X-ray data collection and FT-Raman facility, Vellore Institute of Technology, Vellore for NMR, and CSIR –CECRI, Karaikudi for providing TG/DTA facility.

# Supplementary materials

Supplementary material associated with this article can be found, in the online version, at doi:10.1016/j.chphi.2024.100559.

## References

- [1] S. Singh, From exotic spice to modern drug? Cell 130 (2007) 765–768.
- [2] H.A. Vogel, J. Pelletier, Curcumin-biological and medicinal properties, J. Pharm. 2 (1815) 24–29.
- [3] K. Priyadarsini, The chemistry of curcumin: from extraction to therapeutic agent, Molecules 19 (2014) 20091–20112.
- [4] V. Lampe, J. Milobedzka, V. Kostaneski, Zur Kenntnis des Curcumins, Ber. Deutsch. Chem. Ges. 43 (1910) 2163–2170.
- [5] V. Lampe, J. Milobedzka, Studien über Curcumin, Ber. Deutsch. Chem. Ges. 46 (1913) 2235–2240.

- [6] S.C. Gupta, G. Kismali, B.B. Aggarwal, Curcumin, a component of turmeric: from farm to pharmacy, Biofactors 39 (2013) 2–13.
- [7] T.M. Kolev, E.A. Velcheva, B.A. Stamboliyska, M. Spiteller, DFT and experimental studies of the structure and vibrational spectra of curcumin, Int. J. Quantum. Chem. 102 (2005) 1069–1079.
- [8] S.C. Gupta, S. Prasad, J.H. Kim, S. Patchva, L.J. Webb, I.K. Priyadarsini, B. B. Aggarwal, Multitargeting by curcumin as revealed by molecular interaction studies, Nat. Prod. Rep. 28 (2011) 1937.
- [9] S.C. Gupta, S. Patchva, W. Koh, B.B. Aggarwal, Discovery of curcumin, a component of golden spice, and its miraculous biological activities, Clin. Exp. Pharmacol. Physiol. 39 (2012) 283–299.
- [10] A. Jemal, F. Bray, M.M. Center, J. Ferlay, E. Ward, D. Forman, Global cancer statistics, CA Cancer J. Clin. 61 (2011) 69–90.
- [11] G.B. Rocque, C.P. Williams, K.M. Kenzik, B.E. Jackson, A. Azuero, K.I. Halilova, S. A. Ingram, M. Pisu, A. Forero, S. Bhatia, Concordance with NCCN treatment guidelines: relations with health care utilization, cost, and mortality in breast cancer patients with secondary metastasis, Cancer 124 (2018) 4231–4240.
- [12] P. Vande Perre, D. Toledano, C. Corsini, E. Escriba, M. Laporte, H. Bertet, K. Yauy, A. Toledano, V. Galibert, K. Baudry, L. Clotet, E. Million, M. Picot, D. Geneviève, P. Pujol, Role of the general practitioner in the care of *BRCA1* and *BRCA2* mutation carriers: general practitioner and patient perspectives, Mol. Genet. Genomic. Med. 6 (2018) 957–965.
- [13] M.L. Citron, D.A. Berry, C. Cirrincione, C. Hudis, E.P. Winer, W.J. Gradishar, N. E. Davidson, S. Martino, R. Livingston, J.N. Ingle, E.A. Perez, J. Carpenter, D. Hurd, J.F. Holland, B.L. Smith, C.I. Sartor, E.H. Leung, J. Abrams, R.L. Schilsky, H. B. Muss, L. Norton, Randomized trial of dose-dense versus conventionally scheduled and sequential versus concurrent combination chemotherapy as postoperative adjuvant treatment of node-positive primary breast cancer: first report of intergroup trial C9741/Cancer and Leukemia Group B Trial 9741, J. Clin. Oncol. 21 (2003) 1431–1439.
- [14] J.A. Sparano, M. Wang, S. Martino, V. Jones, E.A. Perez, T. Saphner, A.C. Wolff, G. W. Sledge, W.C. Wood, N.E. Davidson, Weekly paclitaxel in the adjuvant treatment of breast cancer, N. Engl. J. Med. 358 (2008) 1663–1671.
- [15] J.A. Sparano, F. Zhao, S. Martino, J.A. Ligibel, E.A. Perez, T. Saphner, A.C. Wolff, G.W. Sledge, W.C. Wood, N.E. Davidson, Long-term follow-up of the E1199 phase III trial evaluating the role of taxane and schedule in operable breast cancer, J. Clin. Oncol. 33 (2015) 2353–2360.
- [16] G. Kumar Singh, J. Bajpai, S. Joshi, K. Prabhash, A. Choughule, A. Patil, S. Gupta, R. Achyut Badwe, Excellent response to erlotinib in breast carcinoma with rare EGFR mutation—A case report, Ecancermedical science 14 (2020).
- [17] Hassan, Chemotherapy for breast cancer (Review), Oncol. Rep. 24 (2010).
- [18] G.P. Nagaraju, S. Aliya, S.F. Zafar, R. Basha, R. Diaz, B.F. El-Rayes, The impact of curcumin on breast cancer, Integrative Biol. 4 (2012) 996–1007.
- [19] A.B. Kunnumakkara, P. Anand, B.B. Aggarwal, Curcumin inhibits proliferation, invasion, angiogenesis and metastasis of different cancers through interaction with multiple cell signaling proteins, Cancer Lett. 269 (2008) 199–225.
- [20] M. John, B. Jose, Epidermal growth factor receptor targeting in cancer, Semin. Oncol. 33 (2006) 369–385.
- [21] H. Masuda, D. Zhang, C. Bartholomeusz, H. Doihara, G.N. Hortobagyi, N.T. Ueno, Role of epidermal growth factor receptor in breast cancer, Breast. Cancer Res. Treat. 136 (2012) 331–345.
- [22] O.P. Sharma, Antioxidant activity of curcumin and related compounds, Biochem. Pharmacol. 25 (1976) 1811–1812.
- [23] A.J. Ruby, G. Kuttan, K. Dinesh Babu, K.N. Rajasekharan, R. Kuttan, Anti-tumour and antioxidant activity of natural curcuminoids, Cancer Lett. 94 (1995) 79–83.
- [24] Y. Sugiyama, S. Kawakishi, T. Osawa, Involvement of the β-diketone moiety in the antioxidative mechanism of tetrahydrocurcumin, Biochem. Pharmacol. 52 (1996) 519–525
- [25] R.C. Srimal, B.N. Dhawan, Pharmacology of diferuloyl methane (curcumin), a nonsteroidal anti-inflammatory agent, J. Pharm. Pharmacol. 25 (2011) 447–452.
- [26] Y. Hussain, W. Alam, H. Úllah, M. Dacrema, M. Daglia, H. Khan, C.R. Arciola, Antimicrobial potential of curcumin: therapeutic potential and challenges to clinical applications, Antibiotics 11 (2022) 322.
- [27] M. Tomeh, R. Hadianamrei, X. Zhao, A review of curcumin and its derivatives as anticancer agents, Int. J. Mol. Sci. 20 (2019) 1033.
- [28] R. Kuttan, P. Bhanumathy, K. Nirmala, M.C. George, Potential anticancer activity of turmeric (Curcuma longa, Cancer Lett. 29 (1985) 197–202.
- [29] Y. Kiso, Y. Suzuki, N. Watanabe, Y. Oshima, H. Hikino, Antihepatotoxic principles of curcuma longa rhizomes, Planta Med. 49 (1983) 185–187, https://doi.org/ 10.1055/s-2007-969845.
- [30] T. Osawa, Nephroprotective and hepatoprotective effects of curcuminoids, in: 2007: pp. 407–423.
- [31] R. Srivastava, M. Dikshit, R.C. Srimal, B.N. Dhawan, Anti-thrombotic effect of curcumin, Thromb. Res. 40 (1985) 413–417.
- [32] N. Venkatesan, Curcumin attenuation of acute adriamycin myocardial toxicity in rats, Br. J. Pharmacol. 124 (1998) 425–427.
- [33] C. Nirmala, R. Puvanakrishnan, Protective role of curcumin against isoproterenol induced myocardial infarction in rats, Mol. Cell Biochem. 159 (1996) 85–93.
- [34] M. Fu, L. Chen, L. Zhang, X. Yu, Q. Yang, Cyclocurcumin, a curcumin derivative, exhibits immune-modulating ability and is a potential compound for the treatment of rheumatoid arthritis as predicted by the MM-PBSA method, Int. J. Mol. Med. 39 (2017) 1164–1172.
- [35] P. Anand, A.B. Kunnumakkara, R.A. Newman, B.B. Aggarwal, Bioavailability of curcumin: problems and promises, Mol. Pharm. 4 (2007) 807–818.
- [36] M.W. Amolins, L.B. Peterson, B.S.J. Blagg, Synthesis and evaluation of electronrich curcumin analogues, Bioorg. Med. Chem. 17 (2009) 360–367.

- [37] D. Simoni, M. Rizzi, R. Rondanin, R. Baruchello, P. Marchetti, F.P. Invidiata, M. Labbozzetta, P. Poma, V. Carina, M. Notarbartolo, A. Alaimo, N. D'Alessandro, Antitumor effects of curcumin and structurally β-diketone modified analogs on multidrug resistant cancer cells, Bioorg. Med. Chem. Lett. 18 (2008) 845–849.
- [38] B.K. Adams, E.M. Ferstl, M.C. Davis, M. Herold, S. Kurtkaya, R.F. Camalier, M. G. Hollingshead, G. Kaur, E.A. Sausville, F.R. Rickles, J.P. Snyder, D.C. Liotta, M. Shoji, Synthesis and biological evaluation of novel curcumin analogs as anticancer and anti-angiogenesis agents, Bioorg. Med. Chem. 12 (2004) 3871–3883.
- [39] C.A. Mosley, D.C. Liotta, J.P. Snyder, Highly active anticancer curcumin analogues, in: 2007: pp. 77–103.
- [40] H. Bakr El-Nassan, Synthesis and structure activity relationship study of N-substituted 3, 5-diarylidenepiperidin-4-ones as potential antitumor agents, Anti-Cancer Agents Med. Chem. 14 (2014) 319–330 (Formerly Current Medicinal Chemistry-Anti-Cancer Agents).
- [41] G.M. Sheldrick, Program for crystal-structure refinement, SHELX-97, (1997).
- [42] G.M. Sheldrick, SHELXT integrated space-group and crystal-structure determination, Acta Crystallogr. A Found. Adv. 71 (2015) 3–8.
- [43] G.M. Sheldrick, Crystal structure refinement with SHELXL, Acta Crystallogr. C Struct. Chem. 71 (2015) 3–8.
- [44] A.L. Spek, Structure validation in chemical crystallography, Acta Crystallogr. D. Biol. Crystallogr. 65 (2009) 148–155.
- [45] L.J. Farrugia, ORTEP -3 for Windows a version of ORTEP -III with a Graphical User Interface (GUI), J. Appl. Crystallogr. 30 (1997) 565. –565.
- [46] M.J. Turner, J.J. MacKinnon, S.K. Wolff, D.J. Grimwood, P.R.Spackman, D.J, M.A. Spackma. Crystal explorer Ver. 17.5. University of Western Avustralia, Pert. (2017).
- [47] M.K. Priya, D.R. Jonathan, S. Muthu, D.A. Shirmila, J. Hemalatha, G. Usha, Structural examination, theoretical calculations, and pharmaceutical scanning of a new tetralone based chalcone derivative, J. Mol. Struct. 1253 (2022) 132296.
- [48] M.A. Spackman, J.J. McKinnon, D. Jayatilaka, Electrostatic potentials mapped on Hirshfeld surfaces provide direct insight into intermolecular interactions in crystals, CrystEngComm. (2008).
- [49] C.F. Mackenzie, P.R. Spackman, D. Jayatilaka, M.A. Spackman, CrystalExplorer model energies and energy frameworks: extension to metal coordination compounds, organic salts, solvates and open-shell systems, IUCrJ. 4 (2017) 575–587.
- [50] G.M. Morris, D.S. Goodsell, R.S. Halliday, R. Huey, W.E. Hart, R.K. Belew, A. J. Olson, Automated docking using a lamarckian genetic algorithm and empirical binding free energy function, J. Comput. Chem. 19 (1998) 1639–1662.
- [51] The PyMOL Molecular Graphics System, LLC, Schrodinger, 2009, Version 1 5.0.4.
- [52] J. Stamos, M.X. Sliwkowski, C. Eigenbrot, Structure of the epidermal growth factor receptor kinase domain alone and in complex with a 4-anilinoquinazoline inhibitor, J. Biol. Chem. 277 (2002) 46265–46272.
- [53] H.M. Berman, The protein data bank, Nucleic. Acids Res. 28 (2000) 235-242.
- [54] N.M. O'Boyle, M. Banck, C.A. James, C. Morley, T. Vandermeersch, G. R. Hutchison, Open Babel: an open chemical toolbox, J. Cheminform, 3 (2011) 33.
- [55] H.H.F. Refsgaard, B.F. Jensen, P.B. Brockhoff, S.B. Padkjær, M. Guldbrandt, M. S. Christensen, In silico prediction of membrane permeability from calculated molecular parameters, J. Med. Chem. 48 (2005) 805–811, https://doi.org/10.1021/jm049661n.
- [56] S.R. Dasari, S. Tondepu, L.R. Vadali, M.N. Ganivada, N. Seelam, Retracted: synthesis, molecular properties, and biological evaluation of hybrid 1,2,3-triazolylpolyaza heterocyclic compounds, J. Heterocycl, Chem. 56 (2019) 195–208.
- [57] Molinspiration Cheminformatics, novaulica, SK-90026, Slovak Republic. Available from http://www.molinspiration.com. (2021).
- [58] A. Daina, O. Michielin, V. Zoete, SwissADME: a free web tool to evaluate pharmacokinetics, drug-likeness and medicinal chemistry friendliness of small molecules, Sci. Rep. 7 (2017) 42717.
- [59] T. Mosmann, Rapid colorimetric assay for cellular growth and survival: application to proliferation and cytotoxicity assays, J. Immunol. Methods 65 (1983) 55–63.
- [60] K. Prathebha, D. Reuben Jonathan, S. Sathya, J. Jovita, G. Usha, Crystal structure of 4-chloro- N -{[1-(4-chlorobenzoyl)piperidin-4-yl]methyl}benzamide monohydrate, Acta Crystallogr. Sect. E Struct. Rep. Online 70 (2014) o1080-o1080.
- [61] V.N. Nesterov, 3,5-Bis(4-methoxybenzylidene)-1-methyl-4-piperidone and 3,5-bis (4-methoxybenzylidene)-1-methyl-4-oxopiperidinium chloride: potential biophotonic materials, Acta Crystallogr. C 60 (2004) 0806–0809.
- [62] A.I. Almansour, R.S. Kumar, N. Arumugam, R. Vishnupriya, J. Suresh, (3 E,5 E)-1-Allyl-3,5-bis(4-methoxybenzylidene)piperidin-4-one, Acta Crystallogr. Sect. E Struct. Rep. Online 69 (2013) o1071–o1071.
- [63] M. Nardelli, PARST 95 an update to PARST: a system of Fortran routines for calculating molecular structure parameters from the results of crystal structure analyses, J. Appl. Crystallogr. 28 (1995) 659. –659.
- [64] J.A.P Cremer, General definition of ring puckering coordinates, J. Am. Chem. Soc. 97 (1975) 1354–1358.
- [65] M.C. Etter, J.C. MacDonald, J. Bernstein, Graph-set analysis of hydrogen-bond patterns in organic crystals, Acta Crystallogr. B 46 (1990) 256–262.
- [66] H. Osman, N.H. Idris, E.E. Kamarulzaman, H.A. Wahab, M.Z. Hassan, 3,5-Bis (arylidene)-4-piperidones as potential dengue protease inhibitors, Acta Pharm. Sin. B 7 (2017) 479–484.
- [67] M.V. Makarov, I.L. Odinets, K.A. Lyssenko, E.Yu. Rybalkina, I.V. Kosilkin, M. Yu. Antipin, T.V. Timofeeva, N-alkylated 3,5-bis(arylidene)-4-piperidones. Synthetic approaches, X-ray structure and anticancer activity, J. Heterocycl. Chem. 45 (2008) 729–736.
- [68] B. Yao, N. Li, C. Wang, G. Hou, Q. Meng, K. Yan, Novel asymmetric 3,5-bis(arylidene)piperidin-4-one derivatives: synthesis, crystal structures and cytotoxicity, Acta Crystallogr. C. Struct. Chem. 74 (2018) 659–665.

- [69] J.C. Jebapriya, D. Reuben Jonathan, S.R. Maidur, P. Nallamuthu, P.S. Patil, J. C. Prasana, Crystal structure, synthesis, growth and characterization of a nonlinear chalcone crystal: (2E)-1-(4-chlorophenyl)-3-(4-diethylaminophenyl)-prop-2-en-1-one, J. Mol. Struct. 1246 (2021) 131184.
- [70] M.K. Priya, D. Reuben Jonathan, S. Muthu, B.R. Sivasankaran, G. Usha, Synthesis and chemical exploration of an organic exocyclic chalcone derivative for its therapeutic proficiency against breast cancer, Polycycl. Aromat. Compd. (2022) 1–19.
- [71] M. Kurt, P.C. Babu, N. Sundaraganesan, M. Cinar, M. Karabacak, Molecular structure, vibrational, UV and NBO analysis of 4-chloro-7-nitrobenzofurazan by DFT calculations, Spectrochim. Acta a Mol. Biomol. Spectrosc. 79 (2011) 1162–1170
- [72] O.O. Sonibare, T. Haeger, S.F. Foley, Structural characterization of Nigerian coals by X-ray diffraction, Raman and FTIR spectroscopy, Energy 35 (2010) 5347–5353.
- [73] N. Sundaraganesan, G. Elango, C. Meganathan, B. Karthikeyan, M. Kurt, Molecular structure, vibrational spectra and HOMO, LUMO analysis of 4-piperidone by density functional theory and ab initio Hartree–Fock calculations, Mol. Simul. 35 (2009) 705–713, https://doi.org/10.1080/08927020902873992.
- [74] H. Saleem, A.R. Krishnan, Y. Erdogdu, S. Subashchandrabose, V. Thanikachalam, G. Manikandan, Density functional theory studies on 2,5-bis(4-hydroxy-3-methoxybenzylidene)cyclopentanone, J. Mol. Struct. 999 (2011) 2–9.
- [75] J. Coates, Interpretation of infrared spectra, a practical approach. Encyclopedia of Analytical Chemistry, Wiley, 2000.
- [76] V. Meenatchi, K. Muthu, M. Rajasekar, S.P. Meenakshisundaram, Synthesis, spectral, thermal, optical and theoretical studies of (2E,6E)-2-benzylidene-6-(4methoxybenzylidene)cyclohexanone, Spectrochim. Acta A Mol. Biomol. Spectrosc. 120 (2014) 72–76.
- [77] N. Li, W.Y. Xin, B.R. Yao, C.H. Wang, W. Cong, F. Zhao, H.J. Li, Y. Hou, Q.G. Meng, G.G. Hou, Novel dissymmetric 3,5-bis(arylidene)-4-piperidones as potential antitumor agents with biological evaluation in vitro and in vivo, Eur. J. Med. Chem. 147 (2018) 21–33.
- [78] C. Kucuk, S. Yurdakul, B. Erdem, Experimental and theoretical Fourier transform infrared and Raman spectroscopy, density functional theory, antibacterial activity and molecular docking studies on 1-(4-methoxyphenyl)-1H-imidazole, Chem. Pap. 76 (2022) 2833–2854.
- [79] S.D Gupta, M.A.J. Finnilä, S.S. Karhula, S. Kauppinen, A. Joukainen, H. Kröger, R. K. Korhonen, A. Thambyah, L. Rieppo, S. Saarakkala, Raman microspectroscopic analysis of the tissue-specific composition of the human osteochondral junction in osteoarthritis: a pilot study, Acta Biomater. 106 (2020) 145–155.
- [80] M.K Priya, B.K. Revathi, V. Renuka, P. Samuel Asirvatham, Synthesis, structure elucidation, spectroscopic analysis, thermal and NLO properties of A new piperidine derivative (4-Methylphenyl) (4-methylpiperidin-1-yl) methanone, Ont. Laser. Technol. 111 (2019) 616–622.
- [81] F. Adar, Interpretation of raman spectrum of proteins, Spectroscopy 37 (2) (2022) 9-13, 25.
- [82] B. Kiruba, S. Chidambaravinayagam, Photocrosslinking property of certain synthesized bis(arylidene)cycloalkanone based random copolyesters with computational support and their anticancer study, J. Sci. Res. 14 (2022) 901–915.
- [83] K. Govindarasu, E. Kavitha, G. Sundaraganesan, M. Suresh, Mo Syed, A. Padusha, Synthesis, molecular structure and quantum chemical computational interpretations on (E)-N'-(3, 4-Dimethoxy benzylidene)-nicotinohydrazide monohydrate by DFT-B3LYP and MO2-2X level of calculations; a comparative study, Int. J. Adv. Sci. Eng. 2 (2015) 36–57.

- [84] W. Warsi, S. Sardjiman, S. Riyanto, Synthesis and antioxidant activity of curcumin analogues, J. Chem. Pharm. Res. 10 (2018) 1–9.
- [85] Selvam, Ramachandran & G, Velraj, FT-IR, FT-Raman spectral analysis and density functional theory calculations studies of 3-Chloro-2-nitrobenzyl alcohol, Roman. Rep. Phys. 57 (2012) 1128–1137.
- [86] R.N. Compton, N.I. Hammer, Raman under liquid nitrogen (RUN), J. Phys. Conf. Ser. 548 (2014) 012017.
- [87] D. Reuben Jonathan, E. DravidaThendral, M. Krishna Priya, D. Angeline Shirmila, A. Anish Fathima, R. Yuvashri, G. Usha, Investigations on 3D-structure, properties and antibacterial activity of two new curcumin derivatives, J. Mol. Struct. (2023) 136063.
- [88] K.M. Priyadarshini, A. Chandramohan, G.A. Babu, P. Ramasamy, Synthesis, crystal growth, structural, spectral, optical, thermal and dielectric studies of a new nonlinear optical material: 4-Hydroxy-L-proline-L-tartaric acid (1:1), Solid. State Sci. 28 (2014) 95–102.
- [89] P.K. Sivakumar, S. Kumar, R.M. Kumar, R. Kanagadurai, S. Sagadevan, Studies on growth, spectral, thermal, mechanical and optical properties of 4-bromoanilinium 4-methylbenzenesulfonate crystal: a third order nonlinear optical material, Mater. Res. 19 (2016) 937–941.
- [90] T. Chandra Shekhara Shetty, S. Raghavendra, C.S. Chidan Kumar, S. Naveen, S. R. Maidur, P.S. Patil, S. Chandraju, G.S. Ananthnag, S.M. Dharmaprakash, Crystal structure, Hirshfeld and third-order nonlinear optical properties of 3-(4-dimethylamino)phenyl)-1-(4-methoxyphenyl)prop-2-en-1-one: a potential material for optical limiting applications, Opt. Mater. (Amst) 86 (2018) 138–147.
- [91] C. Baydere, M. Taşçı, N. Dege, M. Arslan, Y. Atalay, I.A. Golenya, Crystal structure and Hirshfeld surface analysis of (E)-2-(2,4,6-trimethylbenzylidene)-3,4dihydronaphthalen-1(2 H)-one, Acta Crystallogr. E Crystallogr. Commun. 75 (2019) 746–750.
- [92] H. DJ. A R. Bairy, C.K. Quah, H.C. Kwong, P.S. Patil, Structural, photoluminescence, physical, optical limiting, and hirshfeld surface analysis of polymorphic chlorophenyl organic chalcone derivative for optoelectronic applications, J. Mol. Struct. 1232 (2021) 130053.
- [93] V.R. Hathwar, M. Sist, M.R.V. Jørgensen, A.H. Mamakhel, X. Wang, C. M. Hoffmann, K. Sugimoto, J. Overgaard, B.B. Iversen, Quantitative analysis of intermolecular interactions in orthorhombic rubrene, IUCrJ. 2 (2015) 563–574.
- [94] S. Sevvanthi, S. Muthu, M. Raja, Molecular docking, vibrational spectroscopy studies of (RS)-2-(tert-butylamino)-1-(3-chlorophenyl)propan-1-one: a potential adrenaline uptake inhibitor, J. Mol. Struct. 1173 (2018) 251–260.
- [95] D.A Shirmila, D. Reuben Jonathan, M.K Priya, K. Laavanya, J. Hemalatha, G. Usha, Synthesis, structure determination, molecular interaction analysis, molecular docking studies, and anticancer activity investigation of a chalcone derivative: (2E)-2-[(2,4-dimethoxyphenyl)methylidene]-3,4 dihydronaphthalen-1(2H)-one, Mater. Today Proc. 65 (2022) 2506-2514.
- [96] Y.C. Martin, A bioavailability score, J. Med. Chem. 48 (2005) 3164-3170.
- [97] J. Popiół, A. Gunia-Krzyżak, K. Słoczyńska, P. Koczurkiewicz-Adamczyk, K. Piska, K. Wójcik-Pszczoła, D. Żelaszczyk, et al., The involvement of xanthone and (E)cinnamoyl chromophores for the design and synthesis of novel sunscreening agents, Int. J. Mol. Sci. 22 (1) (2020) 34.
- [98] J. Kalita, D. Chetia, M. Rudrapal, Molecular docking, drug-likeness studies and ADMET prediction of quinoline imines for antimalarial activity, J. Med. Chem. Drug Des. 2 (1) (2019) 1–7.